GDCh Research Article Angewandte International Edition Chemie www.angewandte.org

Check for updates

How to cite: *Angew. Chem. Int. Ed.* **2026**, e22417
doi.org/10.1002/anie.202522417

Batteries Hot Paper

Expediting Desolvation–Diffusion Kinetics by Self-Cascade Catalysis for Durable Low-Temperature Zinc Metal Batteries

Xiaomin Cheng[+], Wenbin Wang[+], Zhiyong Tang[+], Yongzheng Zhang,* Bixian Chen, Jing Zhang, Fangmin Ye, Jing Dong, Hao Li, Jiqiang Jia, Qingbo Xiao, Hongzhen Lin,* and Jian Wang**

Abstract: Dendrite-free Zn metal anodes with robust interface are highly desired for the practical application of aqueous zinc-metal based batteries (AZMBs), while their stability is hindered by the untoward $[Zn(H_2O)_6]^{2+}$ desolvation and succedent deposition with dissatisfactory kinetic barriers, especially under low-temperature environment. Herein, a self-cascade catalytic strategy on accelerating interfacial desolvation and optimizing diffusion is proposed by designing an atomically dispersed Bi within the deficient $LaMnO_{3.15}$ perovskite (SABi/U-LMO) layer on Zn anode. Theoretical calculations demonstrate that the *d*-band center and nonbonding state near the Fermi level of SABi/U-LMO alleviate the corrosion of H_2O and accelerate the dissociation of Zn^{2+}—H_2O bond by promoting the rapid filling of the empty 4s orbital of the Zn^{2+}, as revealed by electrochemical and spectroscopic results. Meanwhile, the redistribution of electric field with SABi/U-LMO realizes the delocalization and lateral growth of Zn atoms. Consequently, the cells with SABi/U-LMO render an impressive lifetime up to 5000 h at 1 mA cm^{-2} as well as a high Coulombic efficiency of 99.59% over 2000 cycles under 0 °C. Full cell also stabilizes the capacity retention of ~100% after 900 cycles at 1 A g^{-1} under −20 °C, verifying the feasibility of self-cascade catalysis in realizing high-performance AZMBs.

Introduction

Aqueous zinc metal batteries (AZMBs), featured by their intrinsically high safety, environmental friendliness and high theoretical specific capacity (820 mAh g^{-1}) of Zn anode, have been widely considered to be one of feasible and reliable energy storage systems.[1–3] However, the stability and durability of AZMBs are far from satisfactory due to the short cycling life and inferior Coulombic efficiency (CE), hindering its practical implementation.[4–6] The underlying mechanism for the depressive performance is associated with the energetical zinc-ion solvation structure ($[Zn(H_2O)_6]^{2+}$), which would not only provoke the hydrogen evolution reactions (HER) with unexpected side reactions but also diverge the zinc-ion fluxes to form uncontrolled Zn dendrites, as illustrated in Figure 1a.[7,8]

As known, the Zn^{2+} plating behavior contains $[Zn(H_2O)_6]^{2+}$ motion in the electrolyte, interfacial desolvation by breaking the Zn^{2+}-H_2O interaction, electrochemical reduction of Zn^{2+} to metastable initial Zn atoms (Zn^0), and finally migration of Zn^0 to potential locations for nucleation, where free Zn^{2+} is both the product

[*] Dr. X. Cheng[+], W. Wang[+], Z. Tang[+], B. Chen, J. Dong, Prof. H. Lin, Dr. J. Wang
i-Lab & CAS Key Laboratory of Nanophotonic Materials and Devices, Suzhou Institute of Nano-Tech and Nano-Bionics, Chinese Academy of Sciences, Suzhou 215123, China
E-mail: xmcheng2023@sinano.ac.cn
hzlin2010@sinano.ac.cn
wangjian2014@sinano.ac.cn
jian.wang@kit.edu

Dr. X. Cheng[+]
Guangdong Institute of Semiconductor Micro-Nano Manufacturing Technology, Guangdong 518103, China

Dr. Y. Zhang
School of Textile & Clothing, Nantong University, Nantong 226019, China
E-mail: zhangyongzheng@ntu.edu.cn

Dr. H. Li, Dr. J. Wang
Helmholtz Institute Ulm (HIU) D89081, Ulm, Germany

Dr. H. Li, Dr. J. Wang
Karlsruhe Institute of Technology (KIT) D76021, Karlsruhe, Germany

Dr. J. Zhang, Dr. J. Jia
School of Materials Science and Engineering, Xi'an University of Technology, Xi'an 710048, China

Dr. F. Ye
Zhejiang Key Laboratory of Quantum State Control and Optical Field Manipulation, Department of Physics, Zhejiang Sci-Tech University, Hangzhou 310018, China

Dr. Q. Xiao
Institute of Agricultural Resources and Environment, Jiangsu Academy of Agricultural Sciences, Nanjing 210014, China

[+] These authors contributed equally to this work.

Additional supporting information can be found online in the Supporting Information section

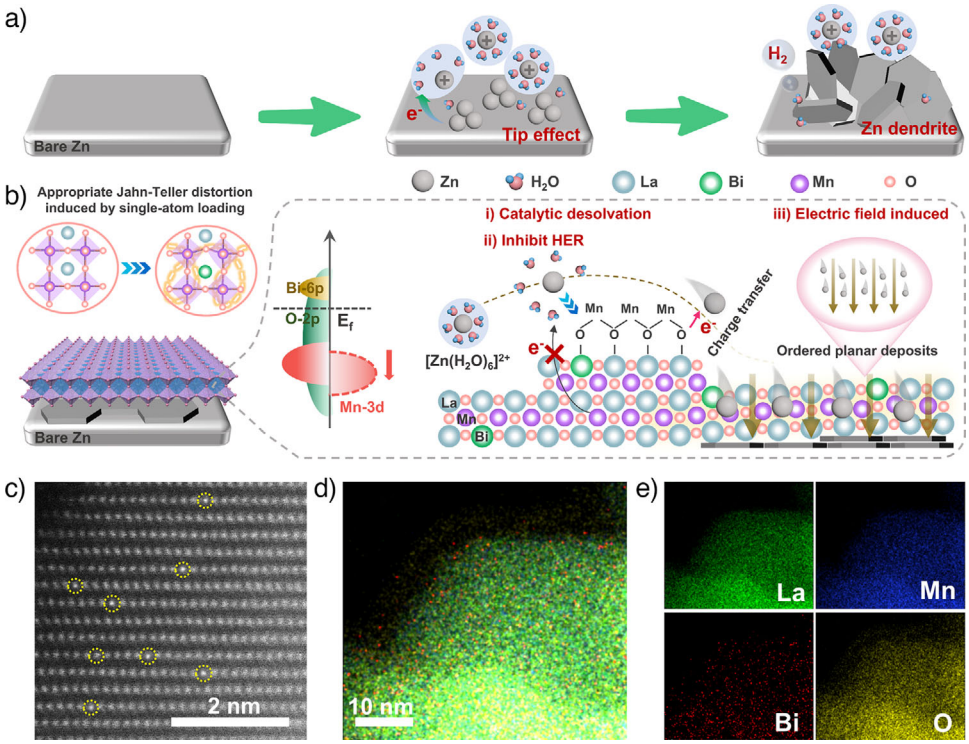

Figure 1. a) Illustration of the zinc ion deposition process. b) Schematic diagram of self-cascade catalytic strategy with tunable electronic structure for zinc ion deposition. c) HAADF-STEM image of SABi/U-LMO. d), e) The corresponding elemental mapping.

of desolvation and the reactant for the subsequent electroreduction to generate Zn^0 for nucleation and growth, exhibiting cascade reaction processes (Figure S1).[9] Among them, the $[Zn(H_2O)_6]^{2+}$ desolvation represents the rate-determining step, exhibiting overwhelming desolvation barriers. Also, the nucleation and growth of Zn^0 are related to the deposition morphology and closely connected with the spatial electric field distribution.[10] The desolvation of $[Zn(H_2O)_6]^{2+}$ and the Zn^0 diffusion and nucleation steps both possess high energy barriers related to the release of the zinc charge carriers from the associated local environment. Currently, great efforts have been made to address these challenges from artificial interface/interphase construction[11,12] to electrolyte optimization,[13–16] among which the electrolyte crowding strategy or the pore screening coupled with chemisorption only focus on the pre-desolvation kinetics, which have not effectively improved the overall reaction kinetics.[11–17] Differing from these engineering, electrocatalytic strategy to precisely control and guide the kinetics of each elementary step in the deposition chain for smooth deposition shows great potential to kinetically modulate these barriers,[18–23] which can simultaneously reduce the desolvation energy barrier and average the subsequently isolated Zn^{2+} flux for reducing diffusion energy barriers.[20] However, the knowledge to realize uniform Zn plating from the aspect of kinetics modulations and the design of ideal space charge regulated self-cascade catalyst has yet to be understood.

Perovskite oxides, a unique 3D electronic structure and flexible intrinsic framework, have attracted wide attention in the fields of electrocatalysis, battery, and superconductivity.[24–26] Inspired by the intrinsic highly active properties of single atoms, the anchoring of heteroatoms on perovskite oxides is proposed to act as a kinetic accelerator to modulate the multidimensional kinetic barriers.[27] And the extra metallic atom-induced charge redistribution is capable of realizing space charge delocalization, effectively evening the distribution of the interfacial electric field.[28] It is expected to achieve the long-life zinc metal battery by leveraging the catalytic desolvation of single atoms and subsequent uniform deposition enabled by redistributed electric field. Currently, however, the atomic-level understanding of the relationship between electronic structure regulation, desolvation and diffusion during the plating process remains largely elusive.

Herein, a novel self-cascade catalytic strategy by designing an atomic bismuth (Bi) distributed defect-rich $LaMnO_{3.15}$ perovskite layer on Zn electrode (SABi/U-LMO@Zn) has been proposed for achieving fast Zn^{2+} desolvation and optimizing subsequent diffusion, acting as cascade catalysts. The falling *d*-band center and a new nonbonding state near the Fermi level (E_f) can promote the fast desolvation of $[Zn(H_2O)_6]^{2+}$ against HER occurrence, as thoroughly confirmed from the electrochemical and spectroscopic characterizations, that is, sum frequency generation spectroscopy (SFG) and Raman to theoretical calculations. Subsequently, the redistribution of electric field with SABi/U-LMO realizes the delocalization and lateral growth of Zn atom. Consequently, the optimal Zn electrodes confer excellent cycling stability over 5000 h at 1 mA cm^{-2} and ultra-stable reversibility with a high average

CE of 99.59% under 0 °C. The assembled full cells with δ-$K_{0.51}V_2O_5$ (KVO) cathodes deliver an excellent cycling performance over 12 000 cycles at 10 A g^{-1} under 0 °C, and a high capacity of 317 mAh g^{-1} without capacity fading at 1 A g^{-1} under −20 °C. This self-cascade catalytic strategy employing atomic catalysts provides a promising path to achieve practical AZMBs.

Results and Discussion

As a prototype, single-atom Bi immobilized on defect-rich $LaMnO_{3.15}$ perovskite was designed to delineate the influence of space charge regulated self-cascade catalyst on the carrier kinetics of each elementary step in the deposition chain, allowing the fast disintegration of the $[Zn(H_2O)_6]^{2+}$ and the subsequent delocalization of Zn atoms (Figure 1b). The fast desolvation kinetics at the interface will also help to avoid HER. As depicted in Figures S2, the samples of LMO, U-LMO and SABi/U-LMO all show uniformly dispersed nanoparticles of ~5 nm. A clear lattice fringe is measured to be around 0.27 nm. The crystallographic structures of the samples were identified by the x-ray diffraction (XRD) Rietveld refinement (Figure S3), which confirms the hexagonal $LaMnO_{3.15}$ perovskite (PDF# 50–0299).[29] The lattice parameters are summarized in Table S1. The slight lattice adjustment without disrupting the crystal structure observed in SABi/U-LMO can induce the appropriate Jahn–Teller distortion, which is beneficial for enhancing electron transfer and catalytic activity.[25] The obtained occupancy results display the higher La vacancies ratio of U-LMO and the ~2 wt% Bi atoms occupancy at the La sites of SABi/U-LMO, confirming the presence of La vacancies on U-LMO and successful synthesis of SABi/U-LMO. The aberration-corrected high-angle annular dark-field scanning transmission electron microscopy (HAADF–STEM) was conducted to characterize the state of atomic Bi. As illustrated in Figures 1c and S4, isolated atomic Bi (highlighted by yellow circles) on the prepared SABi/U-LMO are observed, which is further verified by the atomic mapping in Figure 1d,e.[30] Considering that appropriate Jahn–Teller distortion affects the electronic structure, x-ray photoelectron spectroscopy (XPS) was carried out to discriminate the bonding configuration (Figure S5). In the Mn 2*p* spectrum, the slight shifts toward higher binding energy, and the increased concentration of Mn^{4+} on U-LMO verify the enhanced interaction between Mn and O due to the presence of La vacancies, which is in line with the reported work.[29] With the implantation of atomic Bi, a slight increase in Mn^{3+} concentration is revealed, indicating the charge delocalization.

Density functional theoretical (DFT) calculations were further employed to investigate the evolved electron structure of anchoring atomic Bi on the catalytic desolvation ability and HER inhibition (Figure 2a). As depicted in Figures 2b and S6, the total density of states (TDOS) and projected density of states (PDOS) of SABi/U-LMO show a substantially broadband spanned the E_f with a relatively narrow bandwidth compared to the LMO and U-LMO. Meanwhile, a new spin-polarized nonbonding state near the E_f originated from the Mn 3d-band and O 2p-band (highlighted by dotted lines) appears in SABi/U-LMO compared to the LMO and U-LMO, profoundly uncovering the flexible electronic regulation. For Zn^{2+} reduction, the electronic interaction depends on the lone-pair electrons of substrates to fill the empty 4s orbital of the Zn^{2+} as its 3d orbital is entirely occupied. After adsorbing Zn atoms, the Zn 4s orbital has a high coincidence degree with the orbitals of Mn and Bi atoms in SABi/U-LMO (Figure S7). Combining the Bader charge calculations with charge–density difference maps (Figure S8 and Table S2), it can be concluded that the nonbonding state near the E_f can act as an electron donor to fill the empty 4s orbital of the Zn^{2+}, delivering the fast desolvation and deposition kinetics.[31] The O-2p and Mn-3d band centers are further calculated and the extra Bi atom enables the movement of O-2p band center from −3.60 down to −4.05 eV and the Mn-3d band center from −3.64 down to −4.17 eV, which would contribute to the filled antibonding state with weakened adsorption of H_2O.[32] As shown in Figure 2c, the adsorption energy of H_2O on the SABi/U-LMO is descended compared with LMO, which is consistent with the PDOS results. Strikingly, the adsorption energy of Zn on LMO (1.46 eV) is slightly higher than that on SABi/U-LMO (1.39 eV), but both are far behind that of bare zinc reported in other literature.[33–36] The moderate adsorption energy on SABi/U-LMO is conducive to reducing the diffusion barrier of Zn, benefiting for rapid transport of Zn^{2+} and lateral growth of Zn.[36,37] As confirmed in Figure 2d, the Zn^{2+} diffusion energy barrier within the SABi/U-LMO (0.044 eV) is much lower than that of LMO (0.59 eV). The hydrogen adsorption Gibbs free energy (ΔG_{H^*}) on bare Zn, LMO and SABi/U-LMO are compared to imply the activity of HER (Figure 2e). It is well known that, for HER, the catalytic material with ΔG_{H^*} closer to 0 is the most suitable catalyst.[31] The ΔG_{H^*} values on bare Zn, LMO and SABi/U-LMO are 0.26, −0.56 and 0.99 eV, respectively, showing that the stably H* adsorbed on SABi/U-LMO is difficult to generate and HER is effectively inhibited.[38–40] Based on the above calculations, the falling *d*-band center and a new nonbonding state near the E_f within SABi/U-LMO, facilitated by the strong charge interactions between Bi single atoms and LMO, can effectively modulate the surface adsorption characteristics of Zn and H* species on SABi/U-LMO, which would play a critical role in improving the electrocatalytic desolvation activity and suppressing HER.

As known, the physical properties such as thickness, porosity and surface morphology can affect the ion/atom diffusion and distribution.[41] The cross-sectional scanning electron microscopy (SEM) images of Figure S9 show all elements are well distributed in the SABi/U-LMO@Zn and the best thickness is ~6.7 μm, in which 1.5U-LMO was selected as the catalyst support due to its excellent electrochemical properties (Figure S10). The ionic conductivity of SABi/U-LMO@Zn is calculated to be 11.5 mS cm^{-1}, 3.3 times greater than that of LMO@Zn (Figure S11). Knowing that the interfacial arrangement of cations, anions and water molecules hinges on the properties and local environments of electrode surface, in which the solvated, partially solvated Zn^{2+} dominate the outer Helmholtz layer (OHL), and

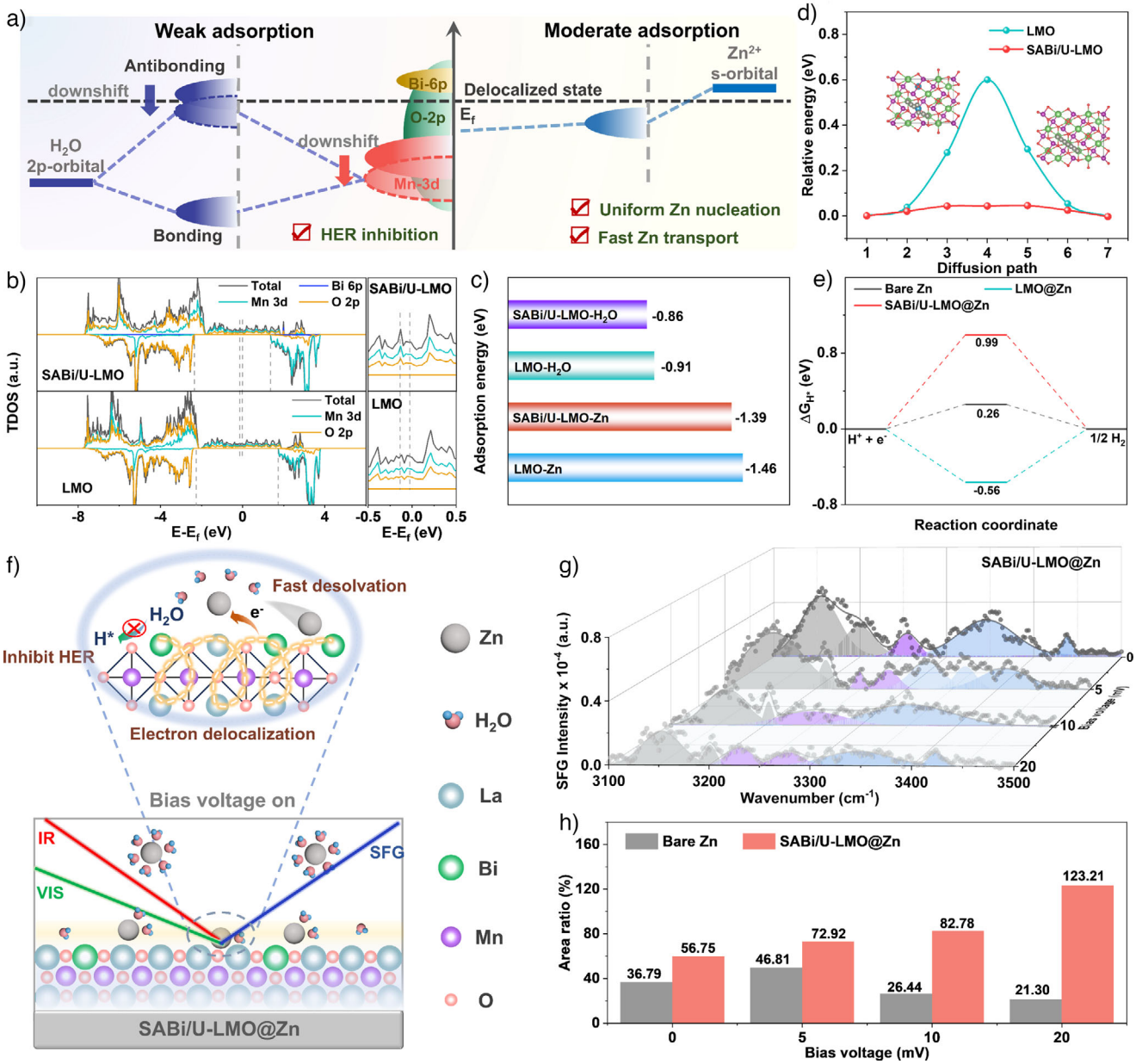

Figure 2. a) Schematic illustration of the adsorption–desorption abilities of H_2O and Zn^{2+} on the SABi/U-LMO layer. b) TDOS of LMO and SABi/U-LMO. c) The adsorption energy of Zn atom and H_2O on LMO and SABi/U-LMO. d) The migration energy of Zn atom transport on LMO and SABi/U-LMO. e) The hydrogen adsorption Gibbs free energy. f) Schematic diagram of the accelerated desolvation of hydrated zinc ions with the bias voltage detected by in-situ SFG. g) The SFG spectra of different states of Zn^{2+} solvation structure under the OH region within the SABi/U-LMO@Zn/electrolyte interface. All spectra have been normalized to their maximum for better visualization. h) The ratio of strongly bound water and loosely bound water.

water dipoles and SO_4^{2-} exist in the inner Helmholtz layer (IHL).[42] The transfer of Zn^{2+} from OHL to IHL, excluding the bound solvated water, is an essential procedure in the Zn plating process.[7] As illustrated in the in-situ SFG of Figure 2f, the desolvation behaviors of the solvated Zn^{2+} at different bias voltages can be dynamically interrogated with the interface-sensitive in-situ SFG via supervising the O—H stretching region at the interface, in which the highly active SABi/U-LMO can break the Zn^{2+}-H_2O bonds and the status of H_2O can be well analyzed.[33,43–46] Three distinct areas with disparate peaks at around 3100–3250, 3250–3300, and 3300–3500 cm^{-1} are observed, which are associated with the O—H features of strongly bound water ("ice-like water"), secondary bond water and loosely bound water ("liquid-like water"), respectively (Figure 2g).[43–45,47] Noting that the intensities of the SFG spectra at the SABi/U-LMO@Zn/electrolyte interface are dramatically weakened and accompanied by a minor red shift compared to that of bare Zn/electrolyte interface at the open circuit voltage (Figure S12), which is related to the redistribution of water

molecules at the interface due to the SABi/U-LMO layer. Upon applying a crescent bias voltage from 0 to 20 mV, more solvated zinc ions are driven to migrate to OHL and undergo desolvation to release Zn^{2+} to participate in the electroreduction reaction, as certified by the substantially decreased SFG intensities.[48,49] Notably, the SFG intensities at the bare Zn/electrolyte interface are more than 10 times stronger than at the SABi/U-LMO@Zn/electrolyte interface regardless of the bias voltage, which is cogently assigned to the catalytic functions of SABi/U-LMO in dissociating the $[Zn(H_2O)_6]^{2+}$. Figure 2h manifests the relative intensity of the free OH peak to the hydrogen-bonded OH peak, which correlates with the structural order of interfacial water. The area ratio at the SABi/U-LMO@Zn/electrolyte interface remains increasing with the increase of bias voltage while that of bare Zn/electrolyte interface first increases and then decreases. These results unravel that the H_2O at bare Zn/electrolyte interface is extremely well ordered, whereas a more random arrangement exists at the SABi/U-LMO@Zn/electrolyte interface during electroreduction.[44] The highly active SABi/U-LMO polarizes the surrounding water molecules, fortifying the proportion of partially solvated Zn ions with a low coordination number of H_2O at SABi/U-LMO@Zn/electrolyte interface.[22]

Raman spectra further verify the remolding of the interaction among anions, cations and H_2O.[50,51] A new peak related to ν-SO_4^{2-} band at 270 cm^{-1} is observed at SABi/U-LMO@Zn/electrolyte interface, assigned to [Zn^{2+}-OSO_3^{2-}], which supports that more OSO_3^{2-} species replace the solvated water to form a more constrict [Zn^{2+}-OSO_3^{2-}] ion association (Figure S13).[52] The desolvation energies (E_a) of $[Zn(H_2O)_6]^{2+}$ are also quantified, and the SABi/U-LMO@Zn electrode delivers the smallest E_a of 16.88 KJ mol^{-1}, verifying a facilitated Zn^{2+} interfacial desolvation (Figure S14).[11] The weakened interaction between Zn^{2+} and the surrounding solvated water derived from the catalytic function of SABi/U-LMO permits Zn^{2+} to escape from the solvation structure easily. As a result, an improved Zn^{2+} transfer number ($t_{Zn^{2+}}$) of SABi/U-LMO@Zn is acquired, 1.4 and 1.9 times greater than that for LMO@Zn and bare Zn electrodes (Figures S15 and S16), respectively.

To clearly capture the contributions of SABi/U-LMO to the interfacial kinetics of the Zn anode and differentiate the elementary reaction steps involved in the plating process, the distribution of relaxation times (DRT) was performed based on the *operando* electrochemical impedance spectra (EIS). As illustrated in Figure 3a–c, four characteristic peaks of reaction process (R_{ad}, $R_{mi\text{-}cr}$, R_{ct}, and R_{diff}) were identified, representing the adsorption of Zn^{2+}, migration of Zn^{2+}/Zn on the surface of Zn crystal and the formation process of crystal Zn, the charge-transfer reaction of Zn^{2+} and subsequent migration through the porous Zn electrode, respectively.[53–56] In contrast to bare Zn and LMO@Zn, R_{ct} of SABi/U-LMO@Zn delivers the smallest τ value of 0.144 s and the weakest peak intensity, indicating the fastest interface reaction kinetics by beefing up desolvation kinetics promoted by SABi/U-LMO layer. Moreover, as depicted in Figure S17, the $\gamma(\tau)$ peaks of the three electrodes shift to the low frequency range with the ceaseless deposition of Zn, in which the peaks of R_{diff} in bare Zn and LMO@Zn appear gigantic shift from 1 to 10 s compared with the SABi/U-LMO@Zn. The huge skewing represents sluggish diffusion kinetics, which may result from the uneven zinc deposition and undesirable by-product formation.[57] Ulteriorly, the evolution of surface morphologies during electroplating process was characterized by in-situ optical microscopy. For the bare Zn, several random aggregations arise only after 20 min, whereas an appreciably sloppy deposition layer with suppressed dendrites is monitored in LMO@Zn (Figure S18). In contrast, the SABi/U-LMO@Zn delivers a denser and smoother deposition layer throughout the entire electroplating process, indicating the delocalization and lateral growth of Zn atom conferred by the redistribution of the interfacial electric field (Figure 3d), which is also confirmed by the SEM (Figures 3e and S19–S21) and chronoamperometry (CA) measurements (Figure S22). Liner sweep voltammetry (LSV) and Tafel curves show that the SABi/U-LMO@Zn possesses the lowest onset potential, the lowest corrosion current density and the highest corrosion potential than bare Zn and LMO@Zn, further confirming the strongly anti-side reaction ability of SABi/U-LMO (Figure S23). Based on the results above, SABi/U-LMO can stabilize electrode/electrolyte interface better by fast desolvation kinetics and uniform deposition.

To trace the stability of SABi/U-LMO and visualize the composition of the interface, symmetrical cells were executed after 25 cycles by the measurement of time-of-flight secondary-ion mass spectroscopy (TOF-SIMS). As elucidated in Figures 3f,g and S24, the cycled SABi/U-LMO@Zn presents lower intensities of the SO^- and ZnO^- species within 500 s compared with that of the bare Zn, which is also displayed in top-view surface mapping and 3D distribution images. Meanwhile, a more random distribution of the ZnO^- species is displayed in bare Zn, while the ZnO^- species in SABi/U-LMO@Zn delivers a more uniform distribution, demonstrating that the SABi/U-LMO layer could uniformize the Zn^{2+} flow and suppress the side reactions. LaO^- and BiO^- species also remain stable on the SABi/U-LMO@Zn after repeated cycling, meaning the stability and applicability of the SABi/U-LMO layer during cycling. Moreover, current density distribution and Zn^{2+} concentration distribution were further monitored by COMSOL to reveal the Zn plating behavior (Figure 3h,i). When the SABi/U-LMO was introduced into the Zn surface, a more homogeneous electric field and Zn^{2+} flux can be achieved, which is quite different from bare Zn, where a heavily accumulated electric field and Zn protrusions with a significant intensity gradient of Zn are found.

Benefiting from the fast desolvation kinetics and self-equalized Zn^{2+} flux enabled by the high catalytic activity of SABi/U-LMO layer, the electrochemical reversibility and stability of zinc anodes are greatly enhanced. As depicted in Figure S25, the SABi/U-LMO@Zn displays the most impressive long-term cyclic stability over 2800 h at 0.2 mA cm^{-2} and 1760 h at 1 mA cm^{-2} with the lowest voltage hysteresis compared to bare Zn and LMO@Zn. It also suggests the stability of SABi/U-LMO during the cycling process. Even at 30 mA cm^{-2} with a high depth of discharge (DOD) of 34%, the cell with SABi/U-LMO@Zn operates stably for over 750 h with a cumulative plated capacity of 9.75 Ah cm^{-2}, while the

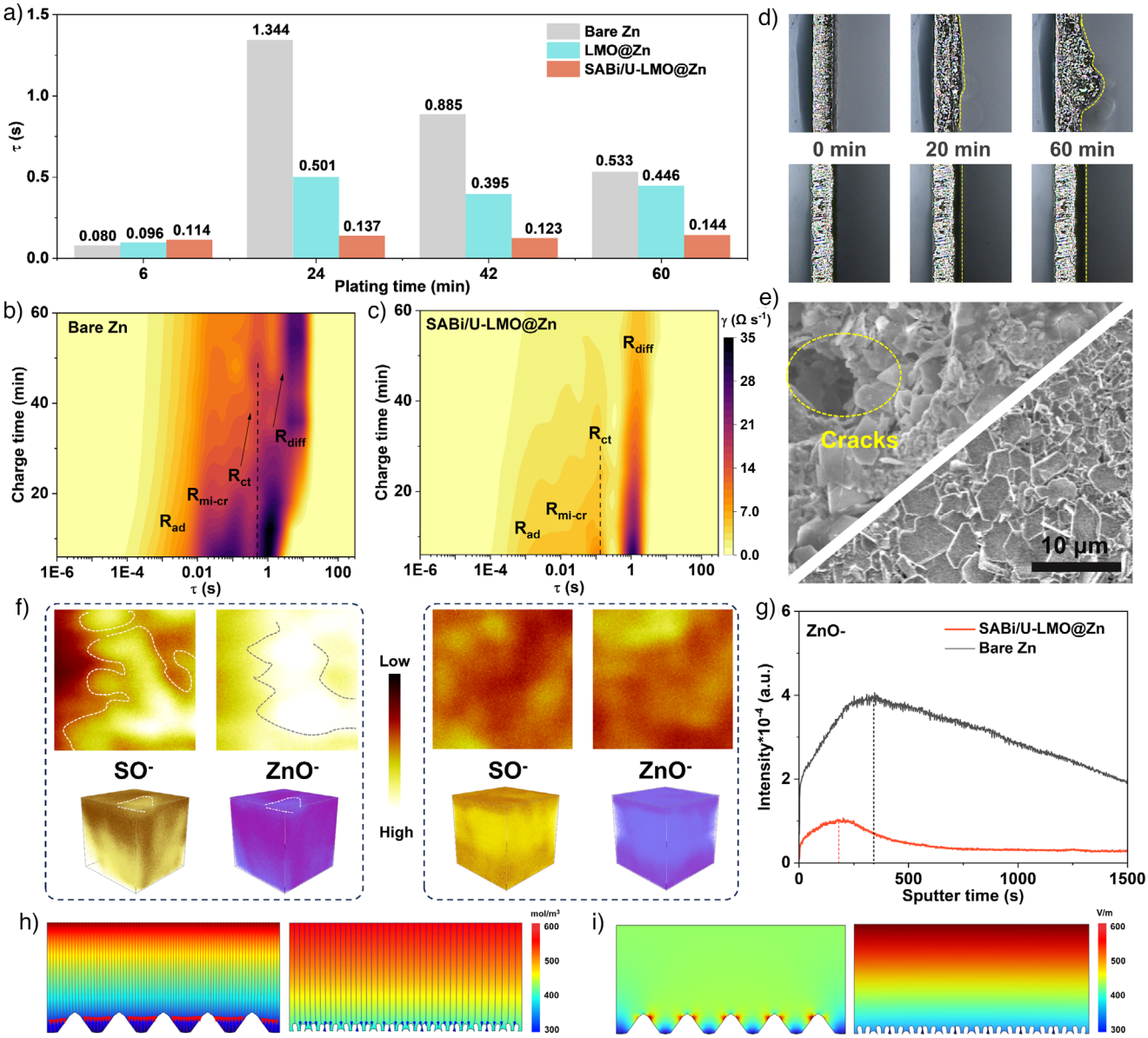

Figure 3. a) The summary of relaxation times of R_{ct} during plating. The distribution of relaxation times (DRT) in b) bare Zn and c) SABi/U-LMO@Zn electrodes. d) In-situ optical microscopic observations of the Zn surface with bare Zn and SABi/U-LMO@Zn electrodes. e) The SEM images of the bare Zn and SABi/U-LMO@Zn electrodes after 25 cycles at 1 mA cm^{-2} and 1mAh cm^{-2}. f) 2D variation and spatial distribution of SO_3^- and ZnO^- on bare Zn (left) and SABi/U-LMO@Zn (right) anodes after 25 cycles. g) Depth profiles of bare Zn and SABi/U-LMO@Zn anodes. h) Simulated Zn^{2+} distribution and i) electric field of bare Zn (left) and SABi/U-LMO@Zn (right) electrodes.

cells with bare Zn and LMO@Zn fail at ~165 and 273 h, respectively. The contrast of Zn plating/stripping stability can be maximized under low-temperature surroundings. A notable contrast in cycling performance is evident, in which a small voltage hysteresis of SABi/U-LMO@Zn from 0.5 to 10 mA cm^{-2} and a low polarization voltage of ~42 mV over 5000 h under 0 °C are shown in Figure S26. Even at a high DOD of 68%, the symmetrical cell with SABi/U-LMO@Zn can be stable for 320 h, surpassing the lifetimes of bare Zn and LMO@Zn (Figure 4a). Moreover, the bare Zn and LMO@Zn show a poor plating/stripping efficiency with an average CE of 99.12% and 99.28% for only 180 cycles and 910 cycles under 0 °C, respectively (Figure S27). Comparatively, the SABi/U-LMO@Zn//Cu cell exhibits an ultrahigh average CE of 99.59% over 2000 cycles with ultra-low overpotential of 136.1 mV (Figure 4b), which can be compared to those coating-engineering Zn anodes (Figure S28). Notably, under -20 °C, the SABi/U-LMO@Zn electrode with $Zn(OTf)_2$ electrolyte still maintains preeminent rate performance and stably runs over 700 h without significant overpotential fluctuations compared to that of bare Zn (Figures 4c and S29). The excellent performance in this work is superior to that in most published works, a comparison presented in Figure 4d and Table S3.

To further validate the feasibility of SABi/U-LMO@Zn in practical application, the full cells were assembled

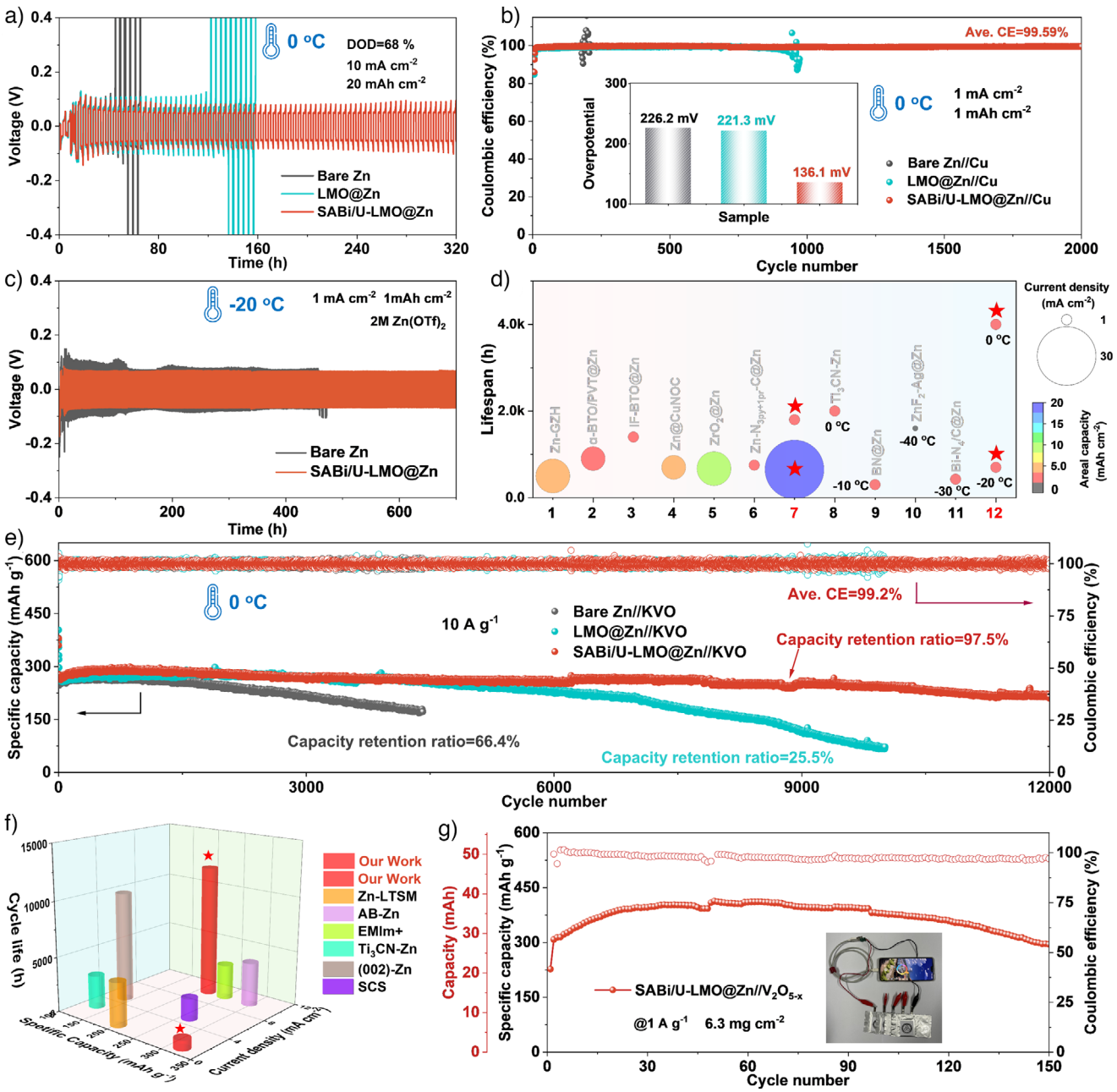

Figure 4. a) Cycling performance of symmetric Zn//Zn cells at 10 mA cm^{-2} for 20 mAh cm^{-2} with high DOD of 68% under 0 °C. b) CE of Zn//Cu cells and corresponding voltage comparison profiles under 0 °C. c) Cycling performance of symmetric Zn//Zn cells using the 2 M $Zn(OTf)_2$ electrolyte under -20 °C with 1 mA cm^{-2} and 1 mAh cm^{-2}. d) Lifespan comparison of this work and the state-of-the-art results reported elsewhere. e) Long-term cycling sustainability under 0 °C with 10 A g^{-1}. f) Performance comparison from previous papers with different modified Zn anodes and our work. g) Cycling performance of SABi/U-LMO@Zn//V_2O_{5-x} pouch cell at 1 A g^{-1} and the photograph of pouch cells for powering a phone.

with KVO cathodes. The as-prepared KVO has a similar microscopic morphology to that in the reported literature (Figure S30).[58,59] The self-discharge curves in Figure S31 show that SABi/U-LMO effectively fortifies the capacity retention ratio, with the CE improved from 86.70% to 95.91%. The cells with SABi/U-LMO@Zn anodes render a longer cycling lifespan of 500 and 5000 cycles at 0.5 A g^{-1} and 5 A g^{-1}, respectively, while the bare Zn//KVO cells fail after 92 and 1500 cycles (Figure S32). Decreasing to 0 °C, the SABi/U-LMO@Zn//KVO cell shows an excellent rate performance from 0.2 to 10.0 A g^{-1}, with the highest discharge capacities ranging from 419 to 281 mAh g^{-1} (Figure S33). Besides, the SABi/U-LMO@Zn//KVO full cell exhibits an excellent cycling performance over 1000 cycles at 0.5 A g^{-1}, compared to the rapid capacity decay for bare Zn//KVO and sudden invalidation at 386 cycles for LMO@Zn//KVO cell (Figure S34). Strikingly, even at 10 A g^{-1}, the SABi/U-LMO@Zn//KVO cell can sustain a high specific capacity of 217 mAh g^{-1} after 12 000 cycles, corresponding to a high retention of 80.3% (Figure 4e). The failure for

LMO@Zn//KVO cell is attributed to the fact that the LMO does not desolvate effectively and therefore cannot afford to work effectively for a long time. When the temperature drops to −20 °C, the SABi/U-LMO@Zn//KVO cell also delivers an outstanding low-temperature tolerance ability with a high specific capacity of 317 mAh g^{-1} after 900 cycles at 1 A g^{-1} (Figure S35). The performance significantly surpasses that of most work, as listed in Figure 4f and Table S4, signifying the significant effect of SABi/U-LMO in regulating desolvation and subsequent migration process. More importantly, the pouch-type SABi/U-LMO@Zn//V_2O_{5-x} cells with large-area electrodes (3.5 × 4 cm^2) were assembled, which renders a high capacity of 296 mAh g^{-1} after 150 cycles at 1 A g^{-1} and enables powering a phone (Figure 4g), confirming the validity and feasibility of the SABi/U-LMO layer for AZMBs.

Conclusion

In summary, a self-cascade catalytic strategy for achieving fast Zn^{2+} desolvation and optimizing Zn atom diffusion is proposed by designing a protective layer on Zn anode composed of atomic Bi anchored on deficient $LaMnO_{3.15}$ perovskite. The atomically dispersed Bi delivers the falling Mn 3*d*-band center and a new nonbonding state near the E_f, modulating the interface electric field. It not only guarantees high reaction activity for fast desolvation of Zn^{2+}, but also realizes the successive delocalization and lateral growth of Zn atom, as comprehensively confirmed by electrochemical analysis, in-situ SFG measurement and theoretical calculations. Benefiting from the boosted kinetics, the SABi/U-LMO@Zn delivers a highly long-lasting Zn plating/stripping behavior with a high CE of 99.59% over 2000 cycles and a high cycling stability of 5000 h at 1 mA cm^{-2} under 0 °C. The optimal low-temperature full cell demonstrates nearly ~100% capacity retention after 900 cycles at 1 A g^{-1} under −20 °C. This new insights into self-cascade catalytic strategy provide fundamental guidance for designing a stable and robust interface.

Acknowledgements

This work was financially supported by the National Key Research and Development Program of China (2021YFA1201503), National Natural Science Foundation of China (No. 22279161, 22572217, and 22309144), China Postdoctoral Science Foundation (No. 2024M762318), Guangdong Basic and Applied Basic Research Foundation (No. 2024A1515110244), Open Project of Inner Mongolia Engineering Research Center of Lithium-Sulfur Battery Energy Storage (No. MDK2025071), Opening funding from Key Laboratory of Engineering Dielectrics and Its Application (No. KFM202507), Ministry of Education) as well as Basic Research Program of Jiangsu (BK20251840). Jian Wang thanks the funding provided by the Alexander von Humboldt Foundation. The authors also thank the support from Nano-X, Suzhou Institute of Nano-tech and Nano-bionics, Chinese Academy of Sciences, and the support from Advanced Materials Analysis and Test Center of Xi'an University of Technology.

Open access funding enabled and organized by Projekt DEAL.

Conflict of Interests

The authors declare no conflict of interest.

Data Availability Statement

The data that support the findings of this study are available from the corresponding author upon reasonable request.

Keywords: Catalytic desolvation · Dendrite-free zinc anode · Self-cascade catalytic strategy · Single atom catalyst · Uniform electric field

[1] Y. Zhang, Z. Cao, S. Liu, Z. Du, Y. Cui, J. Gu, Y. Shi, B. Li, S. Yang, *Adv. Energy Mater.* **2022**, *12*, 2103979, https://doi.org/10.1002/aenm.202103979.

[2] Y. Yang, Z. Tang, S. Bian, Y. Gu, F. Ye, W. Chen, K. Zhu, Y. Wu, L. Hu, *Adv. Energy Mater.* **2025**, *15*, 2500316, https://doi.org/10.1002/aenm.202500316.

[3] L. Jia, H. Hu, X. Cheng, H. Dong, H. Li, Y. Zhang, H. Zhang, X. Zhao, C. Li, J. Zhang, H. Lin, J. Wang, *Adv. Energy Mater.* **2024**, *14*, 2304010, https://doi.org/10.1002/aenm.202304010.

[4] X. Guo, G. He, *J. Mater. Chem. A.* **2023**, *11*, 11987–12001, https://doi.org/10.1039/D3TA01904G.

[5] X. Yu, Z. Li, X. Wu, H. Zhang, Q. Zhao, H. Liang, H. Wang, D. Chao, F. Wang, Y. Qiao, H. Zhou, S.-G. Sun, *Joule* **2023**, *7*, 1145–1175, https://doi.org/10.1016/j.joule.2023.05.004.

[6] J. Zhang, L. Pan, L. Jia, J. Dong, C. You, C. Han, N. Tian, X. Cheng, B. Tang, Q. Guan, Y. Zhang, B. Deng, L. Lei, M. Liu, H. Lin, J. Wang, *Nano Lett.* **2025**, *25*, 3756–3765, https://doi.org/10.1021/acs.nanolett.4c05503.

[7] H. Li, S. Li, R. Hou, Y. Rao, S. Guo, Z. Chang, H. Zhou, *Chem. Soc. Rev.* **2024**, *53*, 7742–7783, https://doi.org/10.1039/D4CS00343H.

[8] Y. Zhang, H. Zhou, J. Gu, H. Yang, X. Cheng, J. Zhang, J. Wang, Y. Wang, H. Lin, J. Wang, L. Zhan, L. Ling, *Energy Storage Mater.* **2025**, *76*, 104161, https://doi.org/10.1016/j.ensm.2025.104161.

[9] W. Wang, J. Dong, H. Hu, X. Cheng, H. Liu, C. Li, Y. Zhang, Q. Guan, H. Li, H. Yang, L. Jia, J. Zhang, H. Lin, J. Wang, *Nano Lett.* **2025**, *25*, 10376–10385, https://doi.org/10.1021/acs.nanolett.5c01731.

[10] J. Wang, J. Zhang, S. Duan, L. Jia, Q. Xiao, H. Liu, H. Hu, S. Cheng, Z. Zhang, L. Li, W. Duan, Y. Zhang, H. Lin, *Nano Lett.* **2022**, *22*, 8008–8017, https://doi.org/10.1021/acs.nanolett.2c02611.

[11] C. Li, X. Cheng, Y. Zhang, J. Zhu, H. Zhou, Y. Yang, J. Xu, J. Wang, Y. Wang, H. Yu, C. Shen, L. Zhan, L. Ling, *J. Colloid Interface Sci.* **2024**, *671*, 505–515, https://doi.org/10.1016/j.jcis.2024.05.202.

[12] W. Xin, J. Xiao, J. Li, L. Zhang, H. Peng, Z. Yan, Z. Zhu, *Energy Storage Mater.* **2023**, *56*, 76–86, https://doi.org/10.1016/j.ensm.2023.01.006.

[13] C. Zhang, J. Holoubek, X. Wu, A. Daniyar, L. Zhu, C. Chen, D. P. Leonard, I. A. Rodríguez-Pérez, J.-X. Jiang, C. Fang, X. Ji,

Chem. Commun. **2018**, *54*, 14097–14099, https://doi.org/10.1039/C8CC07730D.
[14] Q. Zhang, Y. Ma, Y. Lu, L. Li, F. Wan, K. Zhang, J. Chen, *Nat. Commun.* **2020**, *11*, 4463, https://doi.org/10.1038/s41467-020-18284-0.
[15] D. Dong, T. Wang, Y. Sun, J. Fan, Y.-C. Lu, *Nature Sustain.* **2023**, *6*, 1474–1484, https://doi.org/10.1038/s41893-023-01172-y.
[16] K. Guan, W. Chen, Y. Yang, F. Ye, Y. Hong, J. Zhang, Q. Gu, Y. Wu, L. Hu, *Adv. Mater.* **2024**, *36*, 2405889, https://doi.org/10.1002/adma.202405889.
[17] H. Chen, W. Zhang, S. Yi, Z. Su, Z. Zhao, Y. Zhang, B. Niu, D. Long, *Energy Environ. Sci.* **2024**, *17*, 3146–3156, https://doi.org/10.1039/D3EE04333A.
[18] F. Na, X. Li, J. Wang, X. Cheng, J. Zhang, Y. Wang, H. Lin, L. Zhan, L. Ling, Y. Zhang, *Energy Storage Mater.* **2025**, *78*, 104228, https://doi.org/10.1016/j.ensm.2025.104228.
[19] Y. Lin, J. Wang, X. Zhang, X. Cheng, Q. Zhuang, J. Zhang, Q. Guan, Y. Wang, C. Shen, H. Lin, L. Zhan, L. Ling, Y. Zhang, *Adv. Funct. Mater.* **2025**, *35*, 2501496, https://doi.org/10.1002/adfm.202501496.
[20] J. Wang, J. Zhang, Y. Zhang, H. Li, P. Chen, C. You, M. Liu, H. Lin, S. Passerini, *Adv. Mater.* **2024**, *36*, e2402792, https://doi.org/10.1002/adma.202402792.
[21] Q. Guan, J. Wang, Q. Zhuang, J. Zhang, L. Li, L. Jia, Y. Zhang, H. Hu, H. Hu, S. Cheng, H. Zhang, H. Li, M. Liu, S. Wang, H. Lin, *Energy Environ. Sci.* **2024**, *17*, 3765–3775, https://doi.org/10.1039/D3EE04028C.
[22] J. Wang, J. Zhang, J. Wu, M. Huang, L. Jia, L. Li, Y. Zhang, H. Hu, F. Liu, Q. Guan, M. Liu, H. Adenusi, H. Lin, S. Passerini, *Adv. Mater.* **2023**, *35*, 2302828, https://doi.org/10.1002/adma.202302828.
[23] J. Dong, X. Cheng, H. Yang, H. Li, H. Liu, L. Jia, Y. Zhang, Q. Guan, J. Jia, F. Wu, J. Zhang, M. Liu, H. Lin, J. Wang, *Adv. Mater.* **2025**, *37*, e2501079, https://doi.org/10.1002/adma.202501079.
[24] X. Wang, Q. Zhang, X. Li, F. Meng, S. Chen, Z. Chen, Y. Cong, T. Boyko, T. Regier, E. J. Guo, Y. Xiao, L. Li, G. Li, S. Feng, Y. A. Wu, *J. Am. Chem. Soc.* **2024**, *146*, 34364–34373, https://doi.org/10.1021/jacs.4c08643.
[25] Q. Li, J. Wu, T. Wu, H. Jin, N. Zhang, J. Li, W. Liang, M. Liu, L. Huang, J. Zhou, *Adv. Funct. Mater.* **2021**, *31*, 2102002, https://doi.org/10.1002/adfm.202102002.
[26] Z. Wen, Z. Hu, X. Wang, Y. Zhang, W. Du, M. Ye, Y. Tang, X. Liu, C. C. Li, *Adv. Mater.* **2024**, *36*, e2407390, https://doi.org/10.1002/adma.202407390.
[27] J. Wang, J. Zhang, S. Cheng, J. Yang, Y. Xi, X. Hou, Q. Xiao, H. Lin, *Nano Lett.* **2021**, *21*, 3245–3253, https://doi.org/10.1021/acs.nanolett.1c00534.
[28] W. Fan, P. Li, J. Shi, J. Chen, W. Tian, H. Wang, J. Wu, G. Yu, *Adv. Mater.* **2024**, *36*, e2307219, https://doi.org/10.1002/adma.202307219.
[29] X. Liu, J. Mi, L. Shi, H. Liu, J. Liu, Y. Ding, J. Shi, M. He, Z. Wang, S. Xiong, Q. Zhang, Y. Liu, Z. S. Wu, J. Chen, J. Li, *Angew. Chem. Int. Ed.* **2021**, *60*, 26747–26754, https://doi.org/10.1002/anie.202111610.
[30] S. Chen, J. Chen, X. Liao, Y. Li, W. Wang, R. Huang, T. Zhao, S. Yan, Z. Yan, F. Cheng, H. Wang, *ACS Energy Lett.* **2022**, *7*, 4028–4035, https://doi.org/10.1021/acsenergylett.2c02042.
[31] Z. Yang, F. Lai, Q. Mao, C. Liu, R. Wang, Z. Lu, T. Zhang, X. Liu, *Adv. Mater.* **2024**, *36*, 2311637, https://doi.org/10.1002/adma.202311637.
[32] Z. Xu, S. Jin, N. Zhang, W. Deng, M. H. Seo, X. Wang, *Nano Lett.* **2022**, *22*, 1350–1357, https://doi.org/10.1021/acs.nanolett.1c04709.
[33] X. Cheng, Y. Zuo, Y. Zhang, X. Zhao, L. Jia, J. Zhang, X. Li, Z. Wu, J. Wang, H. Lin, *Adv. Sci.* **2024**, *11*, 2401629, https://doi.org/10.1002/advs.202401629.
[34] G. Wang, Q. Yao, J. Dong, W. Ge, N. Wang, Z. Bai, J. Yang, S. Dou, *Adv. Energy Mater.* **2024**, *14*, 2303221, https://doi.org/10.1002/aenm.202303221.
[35] Z. Ge, L. Xu, Y. Xu, J. Wu, Z. Geng, X. Xiao, W. Deng, G. Zou, H. Hou, X. Ji, *Nano Energy* **2024**, *119*, 109053, https://doi.org/10.1016/j.nanoen.2023.109053.
[36] H. Zhang, Y. Wu, J. Yu, T. Jiang, M. Wu, *Adv. Funct. Mater.* **2024**, *34*, 2301912, https://doi.org/10.1002/adfm.202301912.
[37] Y. Meng, M. Wang, J. Xu, K. Xu, K. Zhang, Z. Xie, Z. Zhu, W. Wang, P. Gao, X. Li, W. Chen, *Angew. Chem. Int. Ed.* **2023**, *62*, e202308454, https://doi.org/10.1002/anie.202308454.
[38] R. Deng, Z. He, F. Chu, J. Lei, Y. Cheng, Y. Zhou, F. Wu, *Nat. Commun.* **2023**, *14*, 4981, https://doi.org/10.1038/s41467-023-40462-z.
[39] Z. Shao, L. Lin, W. Zhuang, S. Liu, P. Yang, K. Zhu, C. Li, G. Guo, W. Wang, Q. Zhang, Y. Yao, *Adv. Mater.* **2024**, *36*, 2406093, https://doi.org/10.1002/adma.202406093.
[40] C. Kao, C. Ye, J. Hao, J. Shan, H. Li, S. Qiao, *ACS Nano* **2023**, *17*, 3948–3957, https://doi.org/10.1021/acsnano.2c12587.
[41] M. Huang, K. Guan, B. Chen, Y. Zhang, Y. Liu, K. Miao, H. Lin, P. Wang, X. Cheng, *Adv. Funct. Mater.* **2025**, e25931, https://doi.org/10.1002/adfm.202525931.
[42] L. Jiang, D. Li, X. Xie, D. Ji, L. Li, L. Li, Z. He, B. Lu, S. Liang, J. Zhou, *Energy Storage Mater.* **2023**, *62*, 102932, https://doi.org/10.1016/j.ensm.2023.102932.
[43] S. Yamaguchi, Y. Suzuki, Y. Nojima, T. Otosu, *Chem. Phys.* **2019**, *522*, 199–210, https://doi.org/10.1016/j.chemphys.2019.03.005.
[44] S. Ye, S. Nihonyanagi, K. Uosaki, *Phys. Chem. Chem. Phys.* **2001**, *3*, 3463–3469, https://doi.org/10.1039/b101673n.
[45] H. Wang, W. Chen, J. C. Wagner, W. Xiong, *J. Phys. Chem. B* **2019**, *123*, 6212–6221, https://doi.org/10.1021/acs.jpcb.9b04928.
[46] J. Wang, H. Hu, J. Zhang, L. Li, L. Jia, Q. Guan, H. Hu, H. Liu, Y. Jia, Q. Zhuang, S. Cheng, M. Huang, H. Lin, *Energy Storage Mater.* **2022**, *52*, 210–219, https://doi.org/10.1016/j.ensm.2022.08.004.
[47] T. Li, J. Wang, Y. Xu, Y. Cao, H. Lin, T. Zhang, *ACS Appl. Energy Mater.* **2018**, *1*, 2242–2253, https://doi.org/10.1021/acsaem.8b00321.
[48] J. Zhang, F. Liu, R. He, Q. Guan, N. Tian, J. Wu, Z. Cao, S. Yin, Y. Zhang, L. Jia, X. Li, C. You, H. Liu, M. Liu, Y. Miao, H. Lin, J. Wang, *Adv. Mater.* **2025**, e10894, https://doi.org/10.1002/adma.202510894.
[49] J. Wang, J. Zhang, X. Cheng, Y. Zhang, H. Li, Q. Guan, F. Wu, H. Li, D. Wang, M. Liu, Y. Zhang, Q. Xiao, S. Passerini, H. Lin, *J. Am. Chem. Soc.* **2025**, *147*, 44633–44651, https://doi.org/10.1021/jacs.5c17560.
[50] H. Wang, S. Deng, S. Wang, W. Li, S. Yuan, J. Han, H. Fu, B. Xu, L. Wei, *Angew. Chem. Int. Ed.* **2025**, *64*, e202422395, https://doi.org/10.1002/anie.202422395.
[51] H. Lin, L. Zeng, C. Lin, J. Wu, H. He, C. Huang, W. Lai, P. Xiong, F. Xiao, Q. Qian, Q. Chen, J. Lu, *Energy Environ. Sci.* **2025**, *18*, 1282–1293, https://doi.org/10.1039/D4EE04212C.
[52] H. Yang, Z. Chang, Y. Qiao, H. Deng, X. Mu, P. He, H. Zhou, *Angew. Chem. Int. Ed.* **2020**, *59*, 9377–9381, https://doi.org/10.1002/anie.202001844.
[53] M. Yan, C. Xu, Y. Sun, H. Pan, H. Li, *Nano Energy* **2021**, *82*, 105739, https://doi.org/10.1016/j.nanoen.2020.105739.
[54] L. Wang, B. Zhang, W. Zhou, Z. Zhao, X. Liu, R. Zhao, Z. Sun, H. Li, X. Wang, T. Zhang, H. Jin, W. Li, A. Elzatahry, Y. Hassan, H. Fan, D. Zhao, D. Chao, *J. Am. Chem. Soc.* **2024**, *146*, 6199–6208, https://doi.org/10.1021/jacs.3c14019.
[55] S. Wang, Y. Zhao, H. Lv, X. Hu, J. He, C. Zhi, H. Li, *Small* **2024**, *20*, 2207664, https://doi.org/10.1002/smll.202207664.

[56] J. Zhang, R. He, L. Jia, C. You, Y. Zhang, M. Liu, N. Tian, H. Lin, J. Wang, *Adv. Funct. Mater.* **2023**, *33*, 2305674, https://doi.org/10.1002/adfm.202305674.
[57] S.-M. Lee, J. Kim, J. Moon, K.-N. Jung, J. H. Kim, G.-J. Park, J.-H. Choi, D. Y. Rhee, J.-S. Kim, J.-W. Lee, M.-S. Park, *Nat. Commun.* **2021**, *12*, 39, https://doi.org/10.1038/s41467-020-20297-8.
[58] Y.-H. Zhu, Q. Zhang, X. Yang, E.-Y. Zhao, T. Sun, X.-B. Zhang, S. Wang, X.-Q. Yu, J.-M. Yan, Q. Jiang, *Chem.* **2019**, *5*, 168–179, https://doi.org/10.1016/j.chempr.2018.10.004.
[59] J. Wang, H. Hu, L. Jia, J. Zhang, Q. Zhuang, L. Li, Y. Zhang, D. Wang, Q. Guan, H. Hu, M. Liu, L. Zhan, H. Adenusi, S. Passerini, H. Lin, *InfoMat* **2024**, *6*, e12558, https://doi.org/10.1002/inf2.12558.

Manuscript received: October 13, 2025
Revised manuscript received: December 21, 2025
Manuscript accepted: January 03, 2026
Version of record online: ■■, ■■